Design for a multifrequency high magnetic field superconducting quantum interference device-detected quantitative electron paramagnetic resonance probe: Spin-lattice relaxation of cupric sulfate pentahydrate ($CuSO_4 \cdot 5H_2O$)

Brant Cage[a] and Stephen Russek
National Institute of Standards and Technology, Boulder, Colorado 80305

(Received 7 April 2004; accepted 30 July 2004; published 29 October 2004)

We have designed a spectrometer for the quantitative determination of electron paramagnetic resonance (EPR) at high magnetic fields and frequencies. It uses a superconducting quantum interference device (SQUID) for measuring the magnetic moment as a function of the applied magnetic field and microwave frequency. We used powdered 2,2-diphenyl-1-picrylhydrazyl to demonstrate resolution of g-tensor anisotropy to 1 mT in a magnetic field of 3 T with a sensitivity of 10^{14} spins per 0.1 mT. We demonstrate multifrequency operation at 95 and 141 GHz. By use of an aligned single crystal of cupric sulfate pentahydrate (chalcanthite) $CuSO_4 \cdot 5H_2O$, we show that the spectrometer is capable of EPR line shape analysis from 4 to 200 K with a satisfactory fit to a Lorentzian line shape at 100 K. Below 100 K, we observed line-broadening, g shifts, and spectral splittings, all consistent with a known low-dimensional phase transition. Using SQUID magnetometry and a superconducting magnet, we improve by an order of magnitude the sensitivity and magnetic field range of earlier power saturation studies of $CuSO_4 \cdot 5H_2O$. We were able to saturate up to 70% of the magnetic moment with power transfer saturation studies at 95 GHz, 3.3 T, and 4 K and obtained the spin-lattice relaxation time, $T_1 = 1.8$ ms, of $CuSO_4 \cdot 5H_2O$ at 3.3 T and 4 K. We found an inverse linear dependence of T_1, in units of seconds (s) at 3.3 T between 4 and 2.3 K, such that $T_1 = 0.016 \cdot \mathrm{K} \cdot \mathrm{s} \cdot \tau^{-1} - 0.0022 \cdot \mathrm{s}$, where τ is the absolute bath temperature. The quantitative determination of EPR is difficult with standard EPR techniques, especially at high frequencies or fields. Therefore this technique is of considerable value. [DOI: 10.1063/1.1808893]

I. INTRODUCTION

High-frequency electron paramagnetic resonance (HF–EPR) is proving itself to be a powerful technique for the characterization of magnetic materials.[1–6] It can be used for accurate and sensitive measurements of spin Hamiltonion parameters such as the hyperfine field (A), Lande g tensor (g), which tend to scale as the applied magnetic field (H), spin exchange energy (J), spin–spin interactions due the crystalline field (D), chemical and magnetic structure, electron spin density, spintronic material properties, and evaluation of radiation dosage or dosimetry.[7] There are currently many laboratories that specialize in development of HF–EPR systems,[1–6] and a commercial spectrometer is available operating at 95 GHz. These instruments generally characterize EPR by means of phase-lock detection of radio frequency (rf) fields using Schottky diodes and bolometry, which have inherent problems for quantitative analysis. Here, we describe instrumentation in which EPR is characterized by means of the quantitative observation of the change in magnetic moment due to microwave stimulation using a sensitive magnetometer based on a superconducting quantum interference device (SQUID).

In general, HF–EPR is performed using one of two configurations. In the first,[3,6] the sample is contained within a resonant cavity and the change in quality factor (Q) is measured, from which the imaginary component, χ'', of the microwave susceptibility is determined, or the change in resonant frequency of the cavity is measured from which the real component χ' is derived. The second configuration is a single-pass or transmission measurement where the sample is mounted inside a waveguide and the change in transmitted radiation power is measured as a function of the swept magnetic field.[2,5] The former has the advantage of high sensitivity and discrete observation of χ' and χ'', whereas the latter has the advantage of ease of use, especially for multifrequency measurements. Here we describe a transmission-type approach.

The method uses standard SQUID magnetometry to measure the magnetic moment, expressed as the molar susceptibility χ (in units of $\mathrm{m}^3/\mathrm{mol}$),[8] which, for a paramagnetic material is given by

$$\chi \equiv \frac{M}{H} = \frac{C}{T - \theta}, \tag{1}$$

where M is the molar magnetization in $\mathrm{A\,m^2/mol}$, H is the applied dc magnetic field in A/m, C is the Curie constant in $\mathrm{m^3\,K/mol}$, T is the bath temperature, and θ the Curie–Weiss temperature, both in units of kelvins.

[a]Electronic mail: bcage@boulder.nist.gov

When a paramagnetic sample is illuminated with a continuous-wave rf field the magnetization M decreases near the EPR. The steady-state solution for M is given by the Bloch equation[9]

$$M_Z = M_0 \cdot \frac{1 + (\omega_B - \omega)^2 T_2^2}{1 + (\omega_B - \omega)^2 T_2^2 + (\gamma_e \mu_0 H_1)^2 \cdot T_1 \cdot T_2}, \qquad (2)$$

where $\mu_0 = 4\pi \cdot 10^{-7}$ H/m is the permeability of free space, H_1 is the magnetic component of the microwave excitation field of angular frequency ω, in A/m, γ_e is the gyromagnetic ratio for the electron, in rad s^{-1} T^{-1}, ω_B is the Larmor frequency (angular frequency corresponding to field H), M_0 is the equilibrium magnetization in the presence of a field H, and T_1 and T_2 are, respectively, the longitudinal and transverse relaxation times. Inspection of Eq. (2) indicates that upon application of the H_1 field at resonance, M_Z is reduced by $[1+(\gamma_e \mu_0 H_1)^2 \cdot T_1 \cdot T_2]^{-1}$. Previous experiments[10] that used a vibrating sample magnetometer and a microwave cavity at 14.5 GHz reduced χ by 96% and obtained a value for T_1 of ~40 ms. Here, we build upon this work and use SQUID magnetometry and a superconducting magnet to increase the sensitivity by at least an order of magnitude, a sample the size of 6 mg instead of 100 mg, and an applied magnetic field of 5 T instead of 0.5 T, and examine the field dependence of the spin-lattice relaxation time. There have been experiments using a SQUID to examine the enhanced magnetic relaxation of molecular nanomagnets in a resonant cavity;[11] other work[12] uses a complex setup of micro-Hall bars and a dilution refrigerator at millikelvin temperatures to examine the photon-assisted tunneling of the nanomagnet Fe_8; and very recently, field swept EPR using microsquids at low temperatures <1 K on the $S=1/2$ molecular system V_{15} as well as a preliminary report on Fe_8 at temperatures <1 K.[13,14] The design outlined here uses widely available commercial products to obtain field swept *quantitative* EPR spectra over a large range of temperatures (1.8–200 K), magnetic fields (0–5 T), frequencies (up to 141 GHz) and *explicitly obtains T_1 lifetimes of $S=1/2$ systems as a function of the absorbed microwave power*. Since χ is generally considered to be a bulk parameter, whereas traditional EPR is a local probe, this technique may be complementary to both traditional EPR and susceptibility studies.

II. EXPERIMENT

We used a commercial SQUID magnetometer capable of field sweeps from 0 to 7 T and temperature sweeps of 1.8–400 K. This initial probe design was manufactured with a view to ease of integration into the existing commercial magnetometer. Figure 1 shows the experimental setup. The hollow stainless steel tubing used for sample mounting for susceptibility studies was, in fact, appropriately sized for the 75–110 GHz W band, and calculations determined that the fundamental TE_{11} mode propagates from ~64 to 110 GHz. However, stainless steel is very lossy, so we replaced it with thin-wall round brass tubing, labeled "round waveguide" of the same approximate dimensions (3.175 mm outer diameter by 2.54 mm inner diameter) and 125 cm in length to integrate into the existing system of stepper motor, airlock assembly, cryostat, magnet, and SQUID pickup loops, as labeled. Brass tubing represents a compromise between good microwave transmission and thermal insulation. A homemade transition from coin-silver rectangular V-band WR-15 waveguide to the circular brass waveguide was formed by drilling a 0.125 diameter hole into one end of a 2 in. piece of V-band (50–75 GHz) waveguide with UG-385/U flanges on both ends, and then soldering the brass tube into the drilled hole. This then allows conventional microwave assembly to be mated to the undrilled flanged end. In general, oversized waveguide (hence, the V band, as opposed to W-band fittings) was used for HF–EPR studies to minimize microwave attenuation and allow for a wide frequency range. As shown in Fig. 1, the probe is connected to, by use of flanges, a high frequency >70 GHz microwave source [in this case a 400 mW (as measured by bolometry) 95 GHz or a 141 GHz commercial klystron] through a 95 GHz isolator to prevent reflections into the klystron, a W-band attenuator for saturation studies, and a directional coupler (in this case V band to minimize loss). A detector/mixer at the coupled port monitors the frequency and reflected/incident power. The other end of the three-port directional coupler was connected to the waveguide transition.

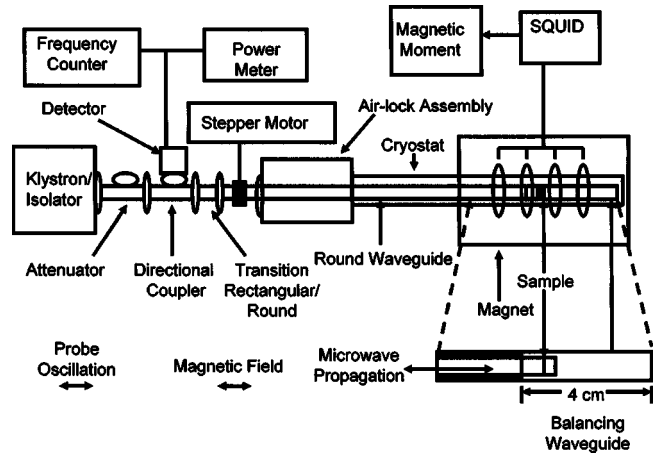

FIG. 1. The experimental setup for quantitative high-field and high-frequency EPR by use of SQUID detection.

The whole probe assembly is mechanically oscillated parallel to the waveguide axis by a stepper motor through the SQUID loops in order to obtain the magnetic moment. The SQUID magnetometer technique is detailed in Ref. 15. Note that this probe design would be effective for basic Faraday extraction of the magnetic moment as well for vibrating-sample magnetometry,[10] which may allow for access to higher magnetic fields.

The background magnetic moment of the probe is 2×10^{-6} A m^2 at 4 K, which is a factor of 30 below that of $CuSO_4 \cdot 5H_2O$. The SQUID magnetometer pickup loops form a second-order gradiometer, and therefore the sample holder, with the sample in the middle, should be homogenous throughout the oscillation length. In order to approximate a uniform background from the waveguide sample holder, we attached an extension tail (labeled balancing waveguide in Fig. 1) to the end of the waveguide.

Figure 1 shows that our measurements utilize the Fara-

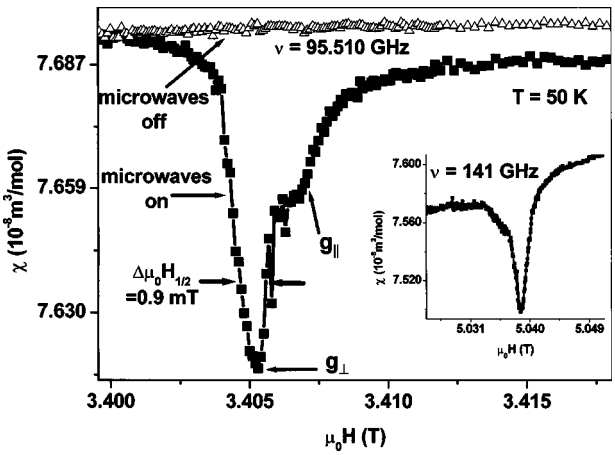

FIG. 2. Magnetic susceptibility, χ, as a function of swept field for a well-ground powder sample DPPH at 50 K. The main figure, triangles (△), show the constant χ. Upon application of 95 GHz microwave stimulation, squares (■), there is a minimum, labeled $g_\perp$, and a minor peak, labeled $g_\parallel$. The inset shows the corresponding χ as a function of swept field at 141 GHz; line broadening appears to reduce the expected enhanced resolution of the g tensor.

day geometry in which the microwave propagation is parallel to the static magnetic field. We currently estimate by means of variable attenuators and a network analyzer that this probe has about 6 dB of attenuation from the source to the sample, which results in 100 mW of power incident on the sample at 95 GHz, at room temperature. The temperature dependence of the attenuation is under investigation. The sample mass for these experiments was 6 mg. The sample filled the entire diameter of the waveguide and was approximately 3 mm in length. The sample oscillation amplitude was 4 cm to minimize line broadening due to magnetic field inhomogeneity. Each value of the magnetic moment was averaged four times at constant field with the magnet in persistent mode. All values of χ to be reported here represent these for the sample and probe, no corrections have been made for background contributions, which results in an estimated absolute error for χ in the second figure for both samples. Further experiments with background subtraction and comparison with conventional SQUID results should dramatically reduce this uncertainty. Our relative resolution of the magnetic moment is at least 5×10^{-9} A m^2 (5×10^{-6} emu).

III. RESULTS AND DISCUSSION

A. Multifrequency quantitative HF–EPR: Powder spectra of DPPH

In Fig. 2 we show quantitative multifrequency HF–EPR by use of SQUID–EPR. For this example we choose the popular commercially available EPR standard 2,2-diphenyl-1-picrylhydrazyl (DPPH) free radical. The utility of DPPH at high fields and frequencies is subject to some debate,[16–18] due, in part, to variations in commercially available DPPH chemical analogs, spectral dependence on chemical preparation (i.e., solvent of recrystallization), and the presence of phase transitions at somewhat high temperatures (10–50 K).[19] We found that our sample, unground, possesses a maximum in the susceptibility at a temperature of about 10 K.

The spin Hamiltonian for DPPH can be represented by

$$H = \mu_B g \cdot \mu_0 H \cdot S + I \cdot A \cdot S, \tag{3}$$

where μ_B is the Bohr magneton, g is the Landé g tensor, H is the applied Zeeman field, S and I are, respectively, the electronic and nuclear spin operators, and A is the hyperfine interaction tensor. In the solid state as a concentrated system, the second term has been shown to be averaged out by spin exchange, so that we are only interested in the field-dependent Zeeman interaction, resulting in the well known resonance condition $h\nu = g\mu_B\mu_0 H$, where h is Planck's constant and ν is the microwave frequency. At low frequencies <20 GHz, a powder sample of DPPH exhibits a single exchange-narrowed line whose width is of the order of 0.1–0.2 mT; for some samples g-tensor anisotropy will result in line structure at higher frequencies.[4,16] In Fig. 2, the triangle data points with no applied microwaves show the expected constant value of χ as a function of magnetic field. Upon microwave irradiation at 95.510 GHz, a minimum and a small shoulder in χ are observed. We attribute this structure to g-tensor anisotropy at 95 GHz and 50 K. We assign the main peak labeled $g_\perp$ to those crystallites whose magnetic axis is perpendicular to the applied field, and assign a minor peak, labeled $g_\parallel$ to those crystallites whose magnetic axis is aligned parallel to the applied Zeeman field. Here, we take $2/3g_\perp + 1/3g_\parallel$ as a field marker to correspond to the X-band isotropic value of $g_{\rm iso}=2.0036$. We then obtain $g_\perp=2.0039$ and $g_\parallel=2.0028$, which is in good agreement with early anisotropic observations[4] at 250 GHz. For a discussion on the behavior of DPPH at high fields please see Ref. 16. The halfwidth (as indicated by the arrows) of the $g_\perp$ transition is 0.9 mT. The signal-to-noise ratio (S/N) defined here as the maximum signal divided by the standard deviation of the baseline, is 12 300. If we define the minimum number of detectable spins as that which gives a S/N of 3:1, then for these conditions, a powder spectrum of lines of 1 mT at 50 K with four scans per point would be 10^{14} spins per 0.1 mT. These data show that 0.0009 T resolution in a 3.3000 T field can be obtained for concentrated spin systems by using this technique. Further experiments utilizing known narrow lines of single aligned crystals at high frequencies would be necessary to determine the absolute resolution and sensitivity at these fields and temperatures.

We investigated whether this technique can yield a corresponding increase in the resolution of the g tensor as described by Eq. (3) at the highest fields. The inset to Fig. 2 shows the EPR spectrum at 141 GHz and 5 T, and we observe a line broadening ($\Delta H_{1/2}=1.8$ mT). Hence, the principal components of the g tensor are not readily differentiated. We mainly attribute this line broadening to field inhomogeneity across the sample path. However, at the least, we have established, a resolution of 0.0018 T in an applied field of 5 T, which is consistent with the specified magnet homogeneity of 10^{-4} parts in 1 cm diameter spherical volume. Single-crystal measurements and smaller scan lengths may improve the resolution at these higher fields.

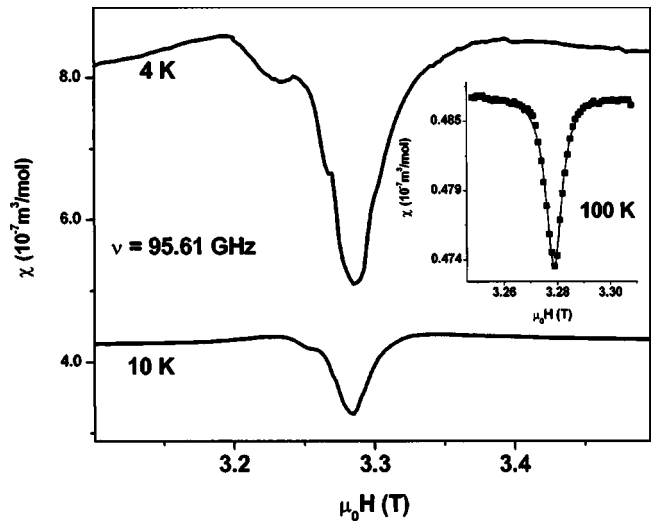

FIG. 3. SQUID–EPR of a single aligned crystal ($g=2.08$) of $CuSO_4 \cdot 5H_2O$ as a function of temperature with $\nu=95.610$ GHz. The main plot, lower to upper, shows that spectral splitting develops as the temperature is lowered from 10 to 4 K. We attribute this to a known low-dimensional phase transition around 1.5 K that removes the magnetic equivalence of the Cu^{++} sublattices. The inset shows a narrow ($\Delta H_{1/2}=7.5$ mT) single peak at 100 K. The squares (■) are the experimental data, and the drawn line is a Lorentzian fit, indicating that this technique is capable of discrete EPR line shape analysis.

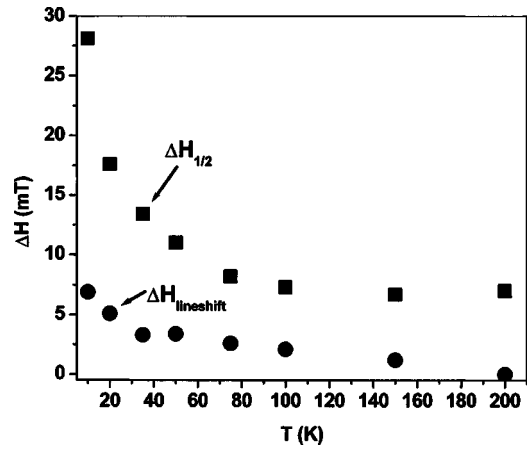

FIG. 4. The temperature dependence of the EPR halfwidth, $\Delta H_{1/2}$, labeled as squares (■), and the relative line-shift ($\Delta H_{1/2}$), indicated by circles (●). These data indicate that this technique is well capable of EPR characterization of an aligned, single, crystal over a wide temperature range.

B. Single-crystal SQUID–EPR of copper sulfate as a function of temperature

In this section we demonstrate that SQUID–EPR is useful as a general HF–EPR tool by characterizing the temperature dependence of the $3d$,[9] $S=1/2$, $CuSO_4 \cdot 5H_2O$ system. The crystal structure[20] indicates that there are two unequivalent Cu^{++} ions in the triclinic unit cell. The geometry of each is nearly octahedral, the structure consisting of four water molecules in a plane and two oxygen atoms; the angle between the planes of water molecules of the two ions is 82°. The Cu^{++} ions form two independent magnetic systems with an exchange interaction of ~10 GHz.[21–23] This results in a single exchange-narrowed line at the X band (~9 GHz), which for the proper orientations[21–23] is then resolved into a doublet at higher frequencies. Here, we orient the crystal such that the copper ions are magnetically equivalent, where the applied magnetic field is perpendicular to both magnetic easy axes.[20–23] The orientation was accomplished by using Refs. 20–23, which outline the crystalline and magnetic structure and iterative adjustments of the crystal orientation until $g_{\perp}=2.08$ was observed. The inset to Fig. 3 shows a single line at 100 K with a linewidth $\Delta H_{1/2}=7.5$ mT. The squares are the data points and the drawn line is a satisfactory fit ($R=0.99$) to a Lorentzian line shape, consistent with the Bloch formalism of Eq. (2). This fit shows that discrete EPR linewidth analysis is achievable by this technique, something that is not so true of conventional HF–EPR transmission studies where admixtures of the real and imaginary components of the alternating current signal render such quantitative studies difficult. The main figure (Fig. 3) shows the EPR at 10 and 4 K. The lines have broadened and begun to split into multiple components. We attribute this to the onset of low-dimensional antiferromagnetic ordering[24] in one of the Cu^{++} sublattices.

Figure 4 shows the linewidth at half-minimum $\Delta H_{1/2}$, of the main peak of copper sulfate as a function of temperature from 200 to 10 K (squares). The linewidth is somewhat constant above 100 K, but begins to broaden below 100 K. The circles in Fig. 4 show corresponding shifts in the resonance position $\Delta H_{\text{line-shift}}$ occur, as a function of decreasing temperature. The observation of broadening and resonance shifts is consistent with the presence of internal demagnetizing fields or short-range order effects preceding a phase transition.[25] These data indicate that this technique is capable of EPR line shape and line-shift analysis as a function of temperature up to at least 200 K.

C. Power transfer studies of T_1 at 3.3 T and 95 GHz

We also built on previous work done by Candela[10] to further characterize the $CuSO_4 \cdot 5H_2O$ system and demonstrate the determination of T_1 by saturation methods using SQUID–EPR at high magnetic fields. The temperature and field dependence of the spin lattice relaxation T_1 are composed of three general mechanisms such that[26]

$$T_1^{-1} = AH^xT + BT^y + C\exp(-\Delta/kT). \tag{4}$$

The first term is the direct process, where the energy emission is through one phonon and x is generally equal to 2 for a non-Kramer's ion (integer spin), or 4 for a Kramer's ion (half-integer spin). The second term is the Raman mechanism, a two-phonon process via an intermediate magnetic ion virtual state, and y can take values of 5, 7, or 9; therefore, this mechanism is dominant at higher temperatures. The third term is the Orbach process where a two-phonon process occurs via a real state with an excitation energy Δ. At low (liquid helium) temperatures the direct process is dominant, and here we adopt the formalism of Candela[10] and Bolger[27] with the assumption that the relaxation process can be described by a single longitudinal relaxation time that is much slower than the transverse relaxation time, T_2, as well as all other processes such as spin exchange, spin diffusion, and lattice-bath heat transfer. Based on these assumptions it has

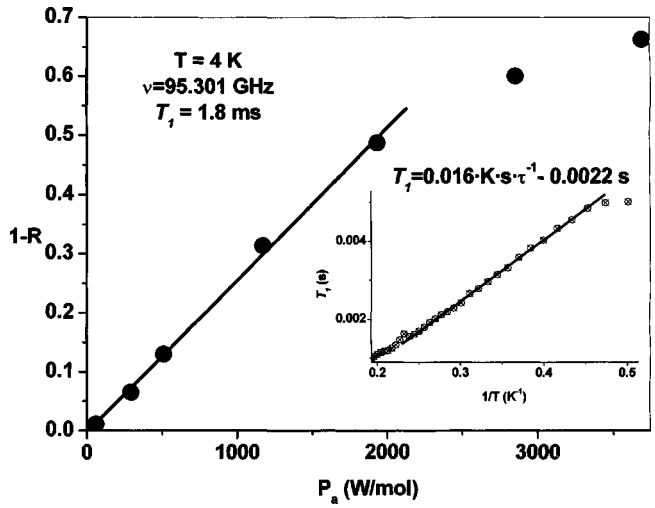

FIG. 5. The degree of saturation $(1-R)$ of $CuSO_4 \cdot 5H_2O$ as a function of the applied microwave ($\nu = 95.301$ GHz) power per mol. The circles (●) are the experimental data, and the drawn line (main figure) is a fit to Eq. (5) that indicates $T_1 = 1.8$ ms at 3.3 T. The inset shows T_1 as a function of inverse temperature over the range 6–2 K. We found an inverse linear dependence of T_1 between 4 and 2.2 K, as expected for a direct process. The drawn line is a fit to Eq. (4).

been shown that T_1, in units of seconds (s), is[10,27]

$$T_1 = \frac{\chi_0 \mu_0 H^2}{P_a}(1-R), \tag{5}$$

where χ_0 is the direct current susceptibility (in units of m^3/mol) in the absence of microwave irradiation, and R is the ratio χ_P/χ_0, with χ_P being the magnetic susceptibility when the sample absorbs microwave irradiation of power P_a (in units of W/mol) at the resonance peak, and H is the applied magnetic field in the z direction, in units of A/m. Figure 5 shows the dependence of the magnitude of (1-R) as a function of the power absorbed (P_a) by the sample for 95 GHz irradiation and 3.3 T applied field. From a fit of the linear region we obtained, $T_1 = 1.8$ ms. Here, with the assumption that the change in reflected power (40%) at resonance relative to off-resonance is indicative of the lower limit of power absorbed, and that the upper limit is the possible power deliverable of 200 mW at 4 K, we use $P_a = 100$ mW, and believe this number is accurate to within a factor of 2–4. The previously determined value[10] of T_1 at 0.5 T and 4 K was 40 ms; therefore these results preliminarily indicate that the field dependence of the lifetime varies as H^{-2}, and not as H^{-4}, which is a surprising result since Cu^{++} is a Kramer's ion, however more data points are needed. Due to the yield of quantitative knowledge of the degree of saturation *at any level*, this technique allows for the evaluation of T_1 in the low-power (linear) saturation regime [see Eq. (5)], whereas conventional EPR studies generally require approaching or exceeding the high-power nonlinear regime. This is important at high frequencies where the available microwave power is usually limited.

Next, we examine the temperature dependence of T_1 at constant power and field. The saturation level was set around 14% at 2 K. This level of saturation is in the linear region of 1-R vs P_a, and this power level minimizes possible crystal heating. The inset to Fig 5 provides the lifetimes as a function of inverse temperature, and, in agreement with earlier work,[10] a linear fit is obtained in the region of 4–2.3 K with a dependence on T_1 of $T_1 = 0.016 \cdot \mathrm{K} \cdot \mathrm{s} \cdot \tau^{-1} - 0.0022 \cdot \mathrm{s}$, where τ is the bath temperature in kelvin, indicating a dominance of the direct relaxation process outlined in Eq. (4). We also investigated (1-R) as a function of temperature at 141 GHz and 5.5 T, and found that T_1 was linear between 2.5 and 4 K and saturation levels of up to 40% were obtainable. These results indicate that this technique is capable of determining the temperature and field dependences of the spin-lattice relaxation time of $S = 1/2$ systems at high magnetic fields and microwave frequencies.

ACKNOWLEDGMENTS

The authors thank Ron Goldfarb for valuable discussions of magnetism and SQUID magnetometry, Denis LaGolvan for determination of the klystron power output, and Bill Riddle, Pavel Kabos, and James Baker-Jarvis for valuable discussions and assistance with the microwave equipment.

[1] B. Cage, A. Hassan, L. Pardi, J. Krzystek, L.-C. Brunel, and N. Dalal, J. Magn. Reson. **124**, 495 (1997).
[2] F. Muller, M. A. Hopkins, N. Coron, M. Grynberg, L. C. Brunel, and G. Martinez, Rev. Sci. Instrum. **60**, 3681 (1989).
[3] S. Hill, N. S. Dalal, and J. S. Brooks, Appl. Magn. Reson. **16**, 237 (1999).
[4] W. B. Lynch, K. A. Earle, and J. H. Freed, Rev. Sci. Instrum. **59**, 1345 (1988).
[5] A. K. Hassan, L. A. Pardi, J. Krzystek, A. Sienkiewicz, P. Goy, M. Rohrer, and L. C. Brunel, J. Magn. Reson. **142**, 300 (2000).
[6] M. Mola, S. Hill, P. Goy, and M. Gross, Rev. Sci. Instrum. **71**, 186 (2000).
[7] F. Callens, G. Vanhaelewyn, and P. Matthys, Spectrochim. Acta, Part A **58**, 1321 (2002).
[8] R. B. Goldfarb and F. R. Fickett, NBS Spec. Publ. 0083-1883 696 (1985); R. L. Sanford and I. L. Cooter, NBS Monogr. 0083-1832 47 (1962).
[9] J. A. Weil, J. R. Bolton, and J. E. Wertz, *Electron Paramagnetic Resonance*, 2nd ed. (Wiley, New York, 1994).
[10] G. A. Candela, J. Chem. Phys. **42**, 113 (1965).
[11] J. Tejeda, R. Amigo, J. M. Hernandez, and E. M. Chudnovsky, Phys. Rev. B **68**, 014431 (2003).
[12] L. Sorace, W. Wernsdorfer, C. Thirion, A.-L. Barra, M. Pacchioni, D. Mailly, and B. Barbara, Phys. Rev. B **68**, 024407 (2003).
[13] W. Wernsdorfer, A. Muller, D. Mailly, and B. Barbara, e-print cond-mat/0404410 (2004); Europhys. J. (to be published).
[14] M. Bal *et al.*, e-print cond-mat/0404448 (2004).
[15] M. McElfresh, *Fundamentals of Magnetism and Magnetic Measurements Featuring Quantum Design's Magnetic Property Measurement System (MPMS), MPMS Application Notes* (Quantum Design, San Diego, CA, 1994).
[16] S. V. Kolaczkowski, J. T. Cardin, and D. E. Budil, Appl. Magn. Reson. **16**, 293 (1999).
[17] N. D. Yordanov, Appl. Magn. Reson. **10**, 339 (1996).
[18] B. Cage, A. Weekley, L.-C. Brunel, and N. Dalal, Anal. Chem. **71**, 1951 (1999).
[19] W. Duffy and D. L. Strandburg, J. Chem. Phys. **46**, 456 (1967).
[20] C. A. Beevers and H. Lipson, Proc. R. Soc. London, Ser. A **46**, 570 (1934).
[21] D. M. S. Bagguley and J. H. E. Griffiths, Proc. R. Soc. London, Ser. A **201**, 366 (1950).
[22] K. Ono and M. Ohtsuka, J. Phys. Soc. Jpn. **13**, 206 (1958).
[23] S. Gharbage, O. F. Meknassi, J.-C. Bissey, and Y. Servant, Physica B **144**, 200 (1987).
[24] S. Wittekoek, N. J. Poulis, and R. Miedema, Physica (Amsterdam) **30**, 1051 (1964).
[25] N. S. Dalal, J. M. Millar, M. S. Jagadeesh, and M. S. Seehra, J. Chem. Phys. **74**, 1916 (1981).
[26] R. L. Carlin and A. J. van Duyneveldt, *Magnetic Properties of Transition Metal Compounds* (Springer, New York, 1977), pp. 35–39.
[27] B. Bolger, Physica (Amsterdam) **26**, 761 (1960), and references therein.